Soft Lag and its Implication of X-ray Time Variation in GRS 1915+105

Yohei Ohkawa and Shunji Kitamoto[1]

Department of Physics, Collage of Science, Rikkyo University, 3-34-1 Nishi-Ikebukuro, Toshima-ku, Tokyo 171-8501, Japan

y-ohkawa@lil.rikkyo.ne.jp, kitamoto@rikkyo.ac.jp

and

Takayoshi Kohmura[1]

Department of General Education, Kogakuin University, 2665-1 Nakano-Cho, Hachioji, Tokyo 192-0015, Japan

tkohmura@map.kogakuin.ac.jp

ABSTRACT

The X-ray time variation of GRS 1915+105 is analyzed, focusing on the phase lag properties in the class θ. The energy dependence and the frequency dependence of the soft lag are derived. This energy dependence can be interpreted by Comptonization of the high energy photons by relatively soft electrons with a temperature of less than $\sim$2 keV. A Monte Carlo simulation of the Comptonization of the power-law photons by soft electrons is presented. This model can explain the energy spectrum, the energy dependence and the frequency dependence of the soft lag. The size of the Compton cloud is estimated to be $\sim 2\times10^9$ cm by comparing the simulation with the data. The time evolution in the class θ including the dip is discussed.

Subject headings: accretion disks — black holes — stars: individual (GRS 1915+105) — X-rays: stars

---

[1]Research Center for Measurement in Advanced Science, Rikkyo University

1. INTRODUCTION

The study of the black hole candidates (BHCs) is now extensively progressing from both observational and theoretical points of view. Especially, the wide band spectral study and the detailed time variation study by *Rossi X-ray Timing Explorer* (*RXTE*) (Bradt, Rothschild, & Swank 1993) exhibited variety of the characteristics of the BHCs. The microquasars make one category among the stellar BHCs, which are characterized by existence of the superluminal jets (Mirabel & Rodríguez 1994) and the very high luminosity of $\sim 5 \times 10^{39} (\mathrm{D}/12\,\mathrm{kpc})^2$ ergs sec^{-1} in the high state (Rau, Greiner, & McCollough 2003). They show lots of interesting phenomena, which must be understood by a general frame work of the accretion disk onto a black hole. Thus, the study of the various behaviors of the microquasars is particularly important for further development of the observational and theoretical understanding of the BHCs.

Majority of the microquasars are X-ray novae. GRS 1915+105 is a unique one which is still active since its discovery in 1992 by the WATCH instrument on-board *GRANAT* (Castro-Tirado, Brandt, & Lund 1992). Especially, this source exhibited many unique behaviors; showing various states and state transitions (Belloni et al. 2000; hereafter B00), absorption lines (Kotani et al. 2000), and quasi-periodic oscillations (QPOs) (Morgan, Remillard, & Greiner 1997) as well as the superluminal jets with the velocity of (0.92 ± 0.08)c (Mirabel & Rodríguez 1994) associating the radio and IR flares (Mirabel et al. 1998). Radio observations of the source showed the distance of 9.0 ± 3.0 kpc in our galaxy (Mirabel & Rodríguez 1994; Fender et al. 1999; Chapuis & Corbel 2004). The binary properties have been also well investigated. It consists of a 14.0 ± 4.4 $\mathrm{M}_\odot$ black hole (Greiner, Cuby, & McCaughrean 2001a; Harlaftis & Greiner 2004) and a 0.81 ± 0.53 $\mathrm{M}_\odot$ K-M III type low mass companion (Greiner et al. 2001b; Harlaftis & Greiner 2004). The orbital period is 33.5 ± 1.5 day (Greiner, Cuby, & McCaughrean 2001a), and its inclination angle is deduced to be 70 ± 2 deg (Mirabel & Rodríguez 1994) or 66 ± 2 deg (Fender et al. 1999).

B00 classified the various states of GRS 1915+105 into twelve classes by the variation of the light curves and the color-color diagrams, and also 3 basic spectral states (A, B, C). The physical interpretation of the complex behaviors and of the connection with the jets is one of the most interesting issues.

Vadawale et al. (2001b; hereafter V01b) analyzed *RXTE* data observed on 1999 June 8 (ObsID : 40702-01-03-00) in order to study the spectral properties of the dips during the radio flare. This observation belongs to the class θ by B00. The class θ consists of low-flux, soft dips (state A in B00) and low-flux, hard intervals (state C in B00). Three component model for the energy spectrum (Rao et al. 2000; Vadawale, Rao, & Chakrabarti 2001a) has been applied, consisting of a disk-blackbody (DiskBB - Mitsuda et al. 1984), a Comptonization

due to hot plasma (CompST - Sunyaev & Titarchuk 1980) and a power-law. During the two dip periods, the QPO is absent (Muno, Morgan, & Remillard 1999; Markwardt, Swank, & Taam 1999; V01b) and the CompST component is very weak (V01b). V01b interpreted that the CompST component disappeared during the dips and this was due to the ejection of the matter in the Compton cloud. This interpretation was supported by the further study of the connection between the radio and X-ray behavior, reported by Vadawale et al. (2003). The temperature of the proposed Compton cloud is several keV. The Compton plasma can be considered to be the inner disk region with the high electron scattering optical depth.

Phase lag has been extensively investigated by Reig et al. (2000) for the low flux intervals (1996 Jul. 11-Aug. 18 and 1997 Sep. 29-Oct. 24). They found that phase lags are present both in the continuum and in the QPO. The sign and the amount of the lag are clearly correlated; the lag is positive (hard lag) when the spectrum is hard and the centroid of the QPO is below 2 Hz. Nobili et al. (2000) interpreted it by the Comptonization model with the corona as formed by the "warm" and "hot" temperature regions. However, the origin of the photons and the size of the cloud are not clear. The study of the time variation must help to understand these questions.

In this paper, we present the results of the analysis of archival *RXTE* data, taking attention to the time variation, especially in the time lag between the various energy bands, with a hope to understand the Comptonized component. A Monte Carlo simulation in order to compare with the observation results is also presented.

2. OBSERVATIONS

GRS 1915+105 is one of the most frequently observed targets by *RXTE*. Vadawale et al. (2003) summarized the connection between the radio flare and the X-ray variability. Among the well related observations, the Proportional Counter Array (PCA) observation, in 1999 June 8 (ObsID : 40702-01-03-00), which shows the typical shape of the radio flare (fast rise and exponential decay), is selected. This observation shows regular cyclic variation including the dips which are considered to relate to the jet ejections. This observation belongs to the class θ.

For the spectral analysis, we analyzed the standard-2 data of PCA and archival data of High Energy X-ray Timing Experiment (HEXTE). For the timing analysis, we used generic binned data with the energy range of 2.15-15.20 keV and the time resolution of 8 m sec. The observed light curve with PCA in the energy range of 2.15-15.20 keV is shown in Figure **??**.

Table 1. Best-Fit Spectral Parameters of The Three Component Model

Regions	$kT_{\rm in}$[a] (keV)	$R_{\rm in}$[b] (km)	$kT_{\rm e}$[c] (keV)	τ[d]	Γ[e]	χ^2 (d.o.f)	2-60 keV Flux $F_{\rm total}$	$F_{\rm diskbb}$	$F_{\rm compst}$	$F_{\rm powerlaw}$
								(10^{-8} ergs s^{-1})		
1a	$1.52^{+0.09}_{-0.07}$	30^{+20}_{-18}	$3.50^{+0.18}_{-0.16}$	> 9.06[f]	$2.90^{+0.06}_{-0.07}$	80 (86)	6.78	1.53	0.81	4.45
1b	$1.56^{+0.10}_{-0.08}$	31^{+20}_{-18}	$4.00^{+0.21}_{-0.18}$	> 6.14[f]	$2.96^{+0.06}_{-0.08}$	77 (86)	7.91	1.94	1.47	4.49
1c	$1.49^{+0.09}_{-0.06}$	47^{+27}_{-26}	$3.34^{+0.28}_{-0.22}$	> 6.64[f]	$2.94^{+0.23}_{-0.33}$	60 (86)	7.41	3.50	1.86	2.08
1d	1.48 ± 0.09	34^{+23}_{-18}	$2.87^{+0.49}_{-0.51}$	> 8.37[f]	$3.45^{+0.45}_{-0.24}$	85 (86)	3.18	1.69	0.24	1.25
1e	$1.55^{+0.11}_{-0.08}$	28^{+18}_{-17}	$3.51^{+0.20}_{-0.17}$	> 7.28[f]	$2.81^{+0.09}_{-0.11}$	42 (86)	5.49	1.46	1.28	2.89
2a	$1.37^{+0.10}_{-0.08}$	26^{+19}_{-18}	$3.85^{+0.34}_{-0.26}$	> 7.95[f]	$2.85^{+0.07}_{-0.08}$	66 (86)	4.28	0.68	0.39	3.22
2b	$1.54^{+0.10}_{-0.08}$	27^{+18}_{-17}	$3.75^{+0.24}_{-0.20}$	> 5.98[f]	2.93 ± 0.06	72 (86)	6.42	1.43	0.69	4.30
2c	$1.42^{+0.10}_{-0.07}$	46^{+28}_{-27}	$2.92^{+0.37}_{-0.27}$	> 6.28[f]	$2.87^{+0.24}_{-0.38}$	59 (86)	5.80	2.68	1.25	1.87
2d	1.47 ± 0.14	35^{+30}_{-22}	$2.37^{+0.51}_{-0.33}$	> 6.06[f]	$3.29^{+0.20}_{-0.26}$	73 (86)	3.61	1.80	0.36	1.45
2e	$1.57^{+0.15}_{-0.11}$	24^{+19}_{-16}	$4.23^{+0.40}_{-0.34}$	> 4.47[f]	$2.81^{+0.11}_{-0.13}$	70 (86)	5.56	1.25	1.14	3.16
3a	$1.41^{+0.15}_{-0.10}$	20^{+17}_{-15}	$4.50^{+0.37}_{-0.31}$	> 5.00[f]	$2.94^{+0.06}_{-0.07}$	87 (86)	3.96	0.47	0.42	3.07

Note. — Errors are 90% confidence levels for a single parameter.

[a]temperature at inner disk radius

[b]inner disk radius. $R_{\rm in}$ is derived from distance D=9.0 kpc and inclination angle $\theta = 70°$.

[c]electron temperature of the Compton cloud

[d]optical depth of the Compton cloud

[e]index of power-law

[f]These are the 90% lower limits.

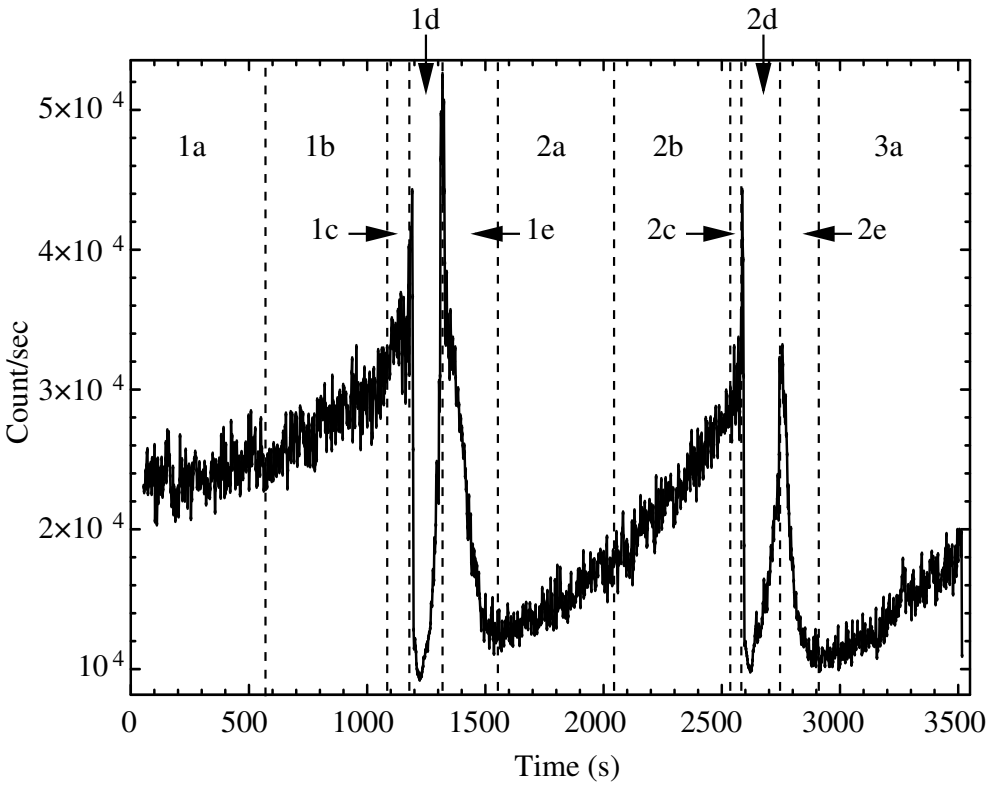

Fig. 1.— PCA light curve in the energy of 2.15-15.20 keV, observed in 1999 June 8.

3. ANALYSIS & RESULTS

3.1. *Energy Spectrum Fitting by The Three Component Model*

The three component model consisting of DiskBB, CompST, and power-law was applied to the data in 1999 June 8 by V01b, where the data were divided into five intervals : pre-pre-dip (1a and 2a, 500s, and 3a, 650s), pre-dip (b, 500s), edge (c, 50s), dip (1d and 2d, 100s and 135s), post-dip (1e, 250s, and 2e, 115s). We also extracted 129 channels spectra from PCA standard-2 data and 64 channels spectra from HEXTE Cluster 0 archival data, and added 2% systematic error for PCA (V01b). We have simultaneously fitted the same three component model to the PCA and HEXTE spectra, in 3-30 keV and in 20-150 keV. First, we kept the $N_{\rm H}$ as a free parameter, but the resultant values of $N_{\rm H}$ and the relating parameters have large errors. Also, the PCA data are not sensitive to the $N_{\rm H}$ values, because we use the data above 3 keV. Thus, we fix the value of $N_{\rm H}$ as the average of the derived values, 7.2×10^{22} H atoms cm^{-1}. This value of $N_{\rm H}$ is slightly larger than 6.0×10^{22} H atoms cm^{-2}, which is used by several authors (Belloni et al. 1997b; Markwardt et al. 1999; Muno et al. 1999; Vadawale et al. 2001). However, other authors used different values; 5.0×10^{22} H atoms cm^{-2} (Rau et al. 2003), 7.0×10^{22} H atoms cm^{-2} (Migliari & Belloni 2003), 12.0-15.0$\times10^{22}$ H atoms cm^{-2} (Vadawale et al. 2003), and etc. These value are ranging between 2.0-15.0$\times10^{22}$ H atoms cm^{-2}, and our value is in this range.

The normalization of the HEXTE spectra with respect to the PCA spectra is dealt with a free parameter. The data are reduced with FTOOLS (Ver. 5.2), and the spectral analysis is performed with XSPEC (Ver. 11.1). The best fit parameters are listed in Table 1, and the model gives reduced χ^2 of order of 1. Figure **??** shows the energy spectrum derived from 2a with PCA and HEXTE, together with the best fit three component model.

From the fitting with the three component model, we confirm the following results. The Comptonizing plasma has the temperature of several keV. The amount of the CompST component during the dip is small. The power-law component decreases during the dips and its index becomes steep. This can not be explained by a simple cloud ejection model. It must be noted that the spectra obtained in the intervals (c) and (e) are some kind of average of the rapidly changing spectra.

3.2. *Short Term Variation*

The results of the spectral fitting suggest the existence of the Comptonized component. In order to confirm this spectral analysis, the study of the short term variation is necessary.

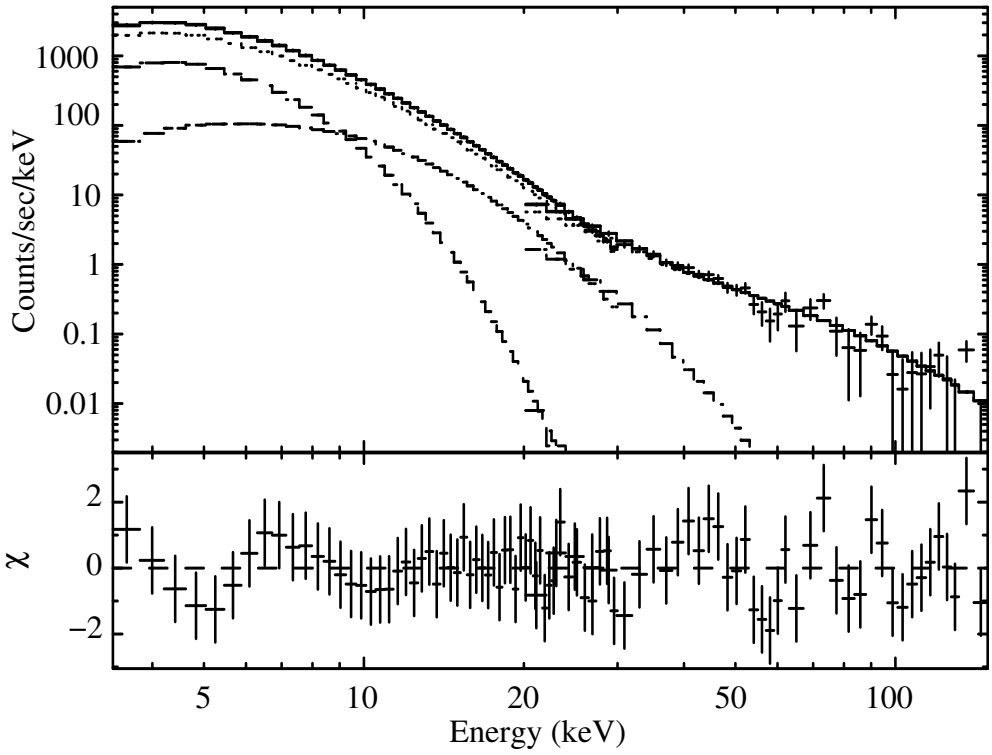

Fig. 2.— Energy spectrum in 2a observed with PCA and HEXTE and the best fit three component model. PCA and HEXTE are covering the energy range of 3-30 keV and 20-150 keV, respectively. The dashed, the dot-dashed, and the dotted curves are the DiskBB, the CompST, and the power-law component, respectively.

Especially, the key to solve the origin of the Comptonized plasma and also the origin of the photons may be derived from the analysis of the short term variation. Thus, we derive the time lag spectra from the cross-spectral analysis. This method was introduced for the investigation of the time variation of the low mass X-ray binaries by van der Klis et al. (1987) and applied to the BHCs by Miyamoto et al. (1988).

We made four light curves in the energy bands (2.15-5.04, 5.04-6.72, 6.72-9.25, 9.25-15.20 keV), and their power spectral densities (PSDs). We also calculated the cross-spectra between the 2.15-5.04 keV energy band and the other energy bands, for the all intervals except for the both sides of the dips (c and e). Figure **??** is the PSD for the 2.15-5.04 keV energy band in 2a and the coherence between 2.15-5.04 keV and 9.25-15.20 keV in 2a. In Figure **??**, we can confirm the 4.89 Hz QPO and the enough high coherence up to 10 Hz.

If we consider the Comptonization of some seed photons, the lag time is expected to be independent on frequency and it has the information of the size of the cloud. An example of the calculated phase lag spectrum of 2a is shown in Figure **??**.

Phase lag around QPO frequency behaves complexly (Lin et al. 2000; Reig et al. 2000). The derived phase lag spectra show apparent linear line crossing the origin in the low frequency range below 2 Hz. However, above 2 Hz, even though excluding QPO frequency (3.68-6.11 Hz), the time lag is not independent on frequency. Very similar phase lag spectra were observed in July 16, 2001 as reported by Vadawale et al. (2003). The frequency dependence of the phase lag is discussed in the next section. By restricting the frequency range below 2 Hz, a linear function is fitted to the data and we derive the delay time with respect to the 2.15-5.88 keV band. The results are summarized in Table **??** and shown in Figure **??** for 2a and 2b. The tendency of the advance of the harder band is clearly seen, in both the intervals; 2a and 2b.

If the Comptonization introduced in the spectral fitting is the inverse Compton scattering by hot electrons (with the temperature of $\sim$4 keV) of soft photons, hard lag is expected. On the other hand, if hard photons are scattered by cold electrons, soft lag is expected in the low energy region. The data show the soft lag suggesting the scattering by rather cold electrons.

3.3. *Comptonized-Powerlaw Model*

The analysis of time lag shows the soft lag in the energy range between 2 keV and 15 keV. The seed photons of the CompST model are low energy photons, thus the soft lag can not be expected. In order to produce the soft lag by the Comptonization, the seed

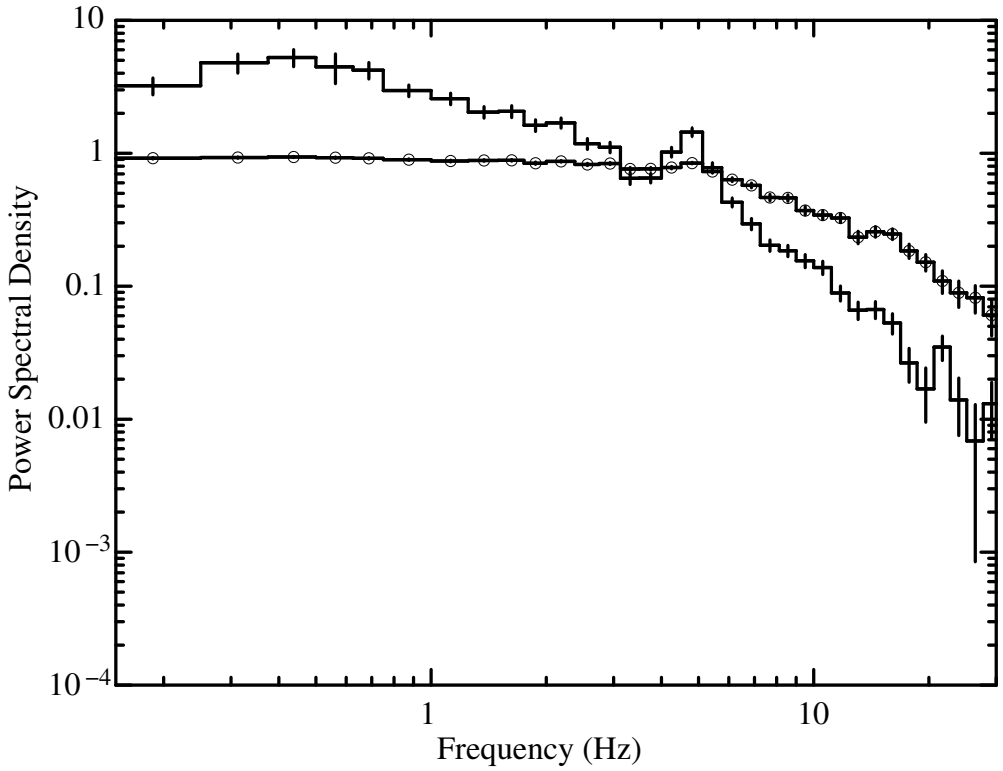

Fig. 3.— Power spectral density of 2.15-5.04 keV energy band (*crosses*) and coherence of 9.25-15.20 keV energy band with respect to the 2.15-5.04 keV energy band (*circles*) in 2a.

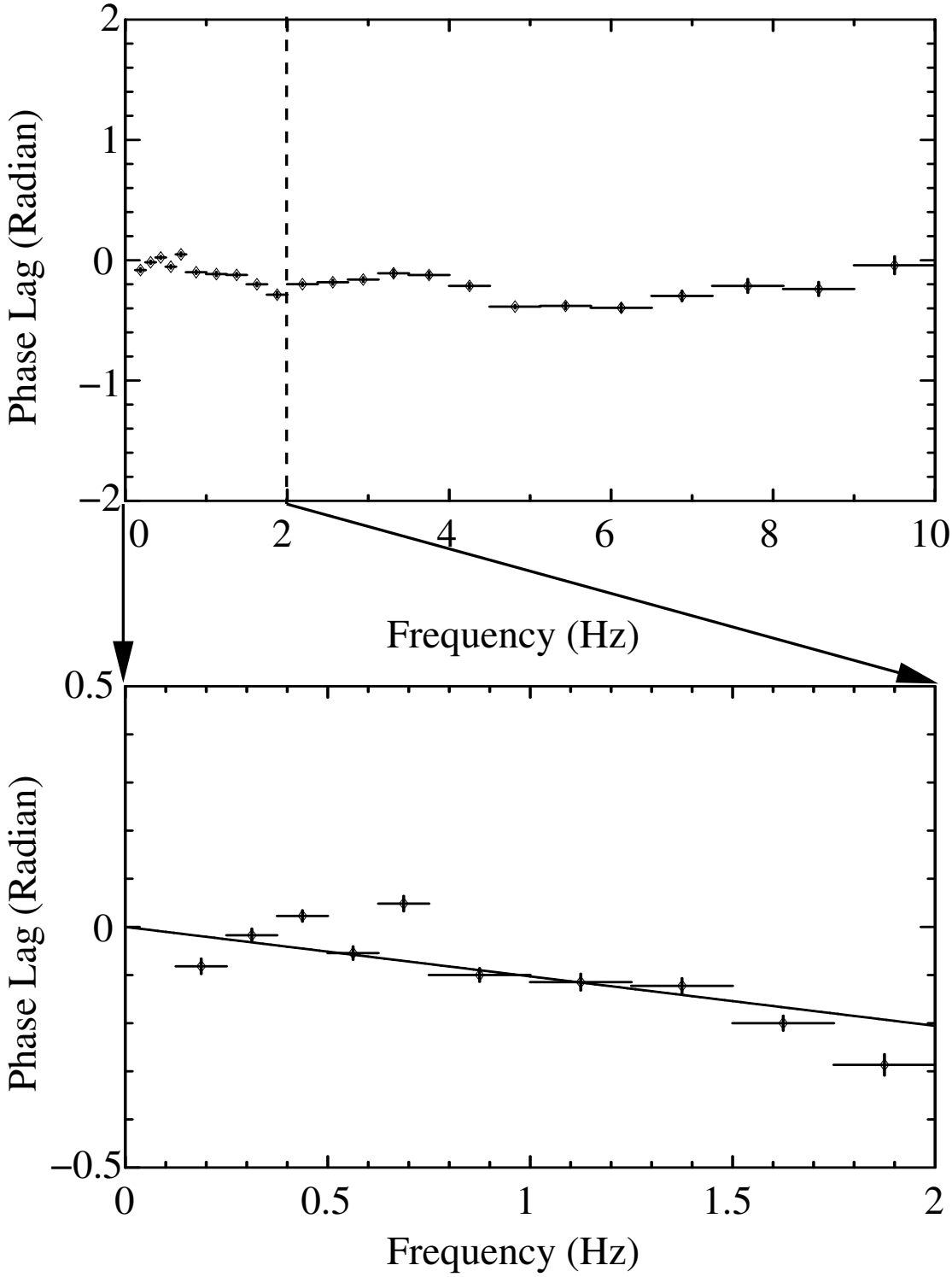

Fig. 4.— Phase lag of the 9.25-15.20 keV energy band with respect to the 2.15-5.04 keV energy band in 2a. The line represents the best-fit to the data.

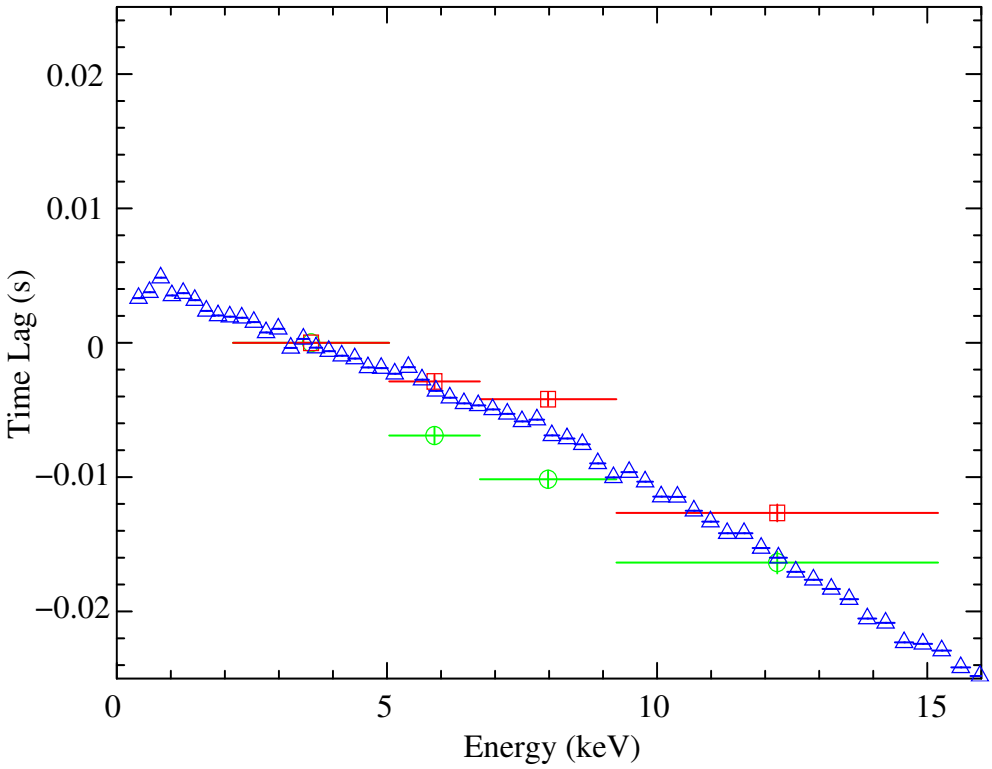

Fig. 5.— Energy dependence of the time lag. Each mark shows the time lag with respect to 2.2-5.0 keV in 2a (*circles*), in 2b (*squares*). The *triangles* show the results of the simulations, where the electron temperature of 0.1 keV, the optical depth of 4 and the plasma radius of 2×10^9 cm are assumed.

photons must be high energy photons. In the observed energy spectra, the hard component is basically the power-law component. Thus, the candidate of the hard seed photons is the power-law component. Here, we construct a Comptonized power-law model by the electrons with the temperature of order of keV.

We assume a Compton cloud is spherically symmetric, and its density and temperature are constant with regard on the radius for simplification, although actual geometry must be complex. The seed photons are originated in the center of the cloud with a power-law spectrum between 0.2 keV and 180 keV. The electrons are assumed to have the Maxwellian distribution. The calculation carried out by the Monte Carlo method. The parameters are the index and the normalization of the power-law, the electron temperature and the optical depth of the plasma. We call this model as Comptonized-Powerlaw (CompPL).

Some examples of the calculated emerging energy spectra divided by the initial energy spectra, for five cases of the electron temperatures, are shown in Figure **??**, where we assume the initial photon index of -2.7 and the electron scattering optical depth of 4. It can be recognized that the photons are concentrating toward the energy of the electrons. The emerging energy spectra are similar to the combination of a simple power-law and a thermal spectrum with the electron temperature.

The calculated spectra are converted to the atable model of XSPEC, and the two component model consisting of DiskBB and CompPL is fitted to the observed spectra. This model can well simulate the data both with the electron temperature of 4-6 keV and less than 2.5 keV. However, in order to satisfy both the spectral data and the time lag data low energy solution is preferable. As an example, the spectrum in 2a is shown in Figure **??** together with the best fit model. We emphasize that the number of parameters of the two component model is fewer than that of the three component model.

The mean escape time with a unit of mean free time, as a function of the energy of the emerging photons, is shown in Figure **??** for five cases of electron temperature, where we again assume the initial photon index of -2.7 and the electron scattering optical depth of 4. In the energy range from 2 keV to 15 keV, if the electron temperature is less than $\sim$2 keV, 2 keV photons take longer escape time than 15 keV photons. Therefore, soft lag is expected. On the other hand, if the electron temperature is greater than 4 keV, hard lag is expected.

The observed frequency dependence of the lag is not simple. The calculated lag is the average of the difference of arguments of the complex Fourier spectra derived from the two light curves. However, the actual data always include the statistical fluctuation. This statistical fluctuation makes the average to be small. Also in the actual data, several spectral components are combined and the derived lag is affected by all the components (Kohmura,

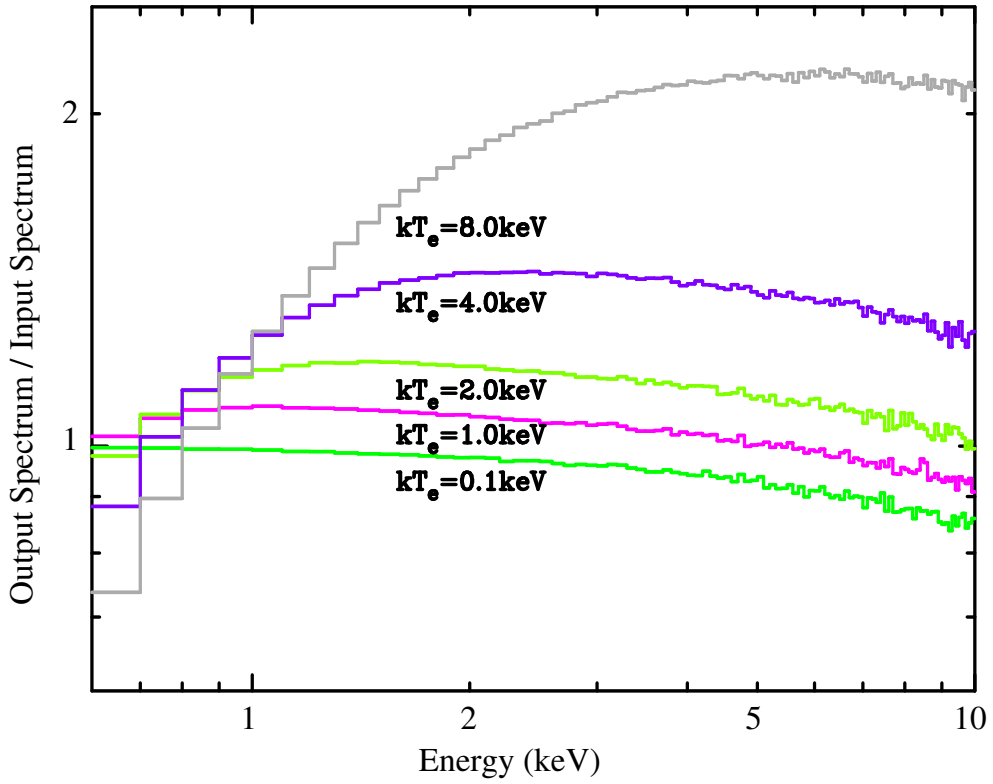

Fig. 6.— Change of the spectra by the Comptonization. The initial spectra are assumed to be a power-law with the photon index of -2.7, and the optical depth of the plasma is 4. The ratios of the spectra of the emerging photons to that of the incident photons are plotted. The assumed electron temperatures are indicated in the figure.

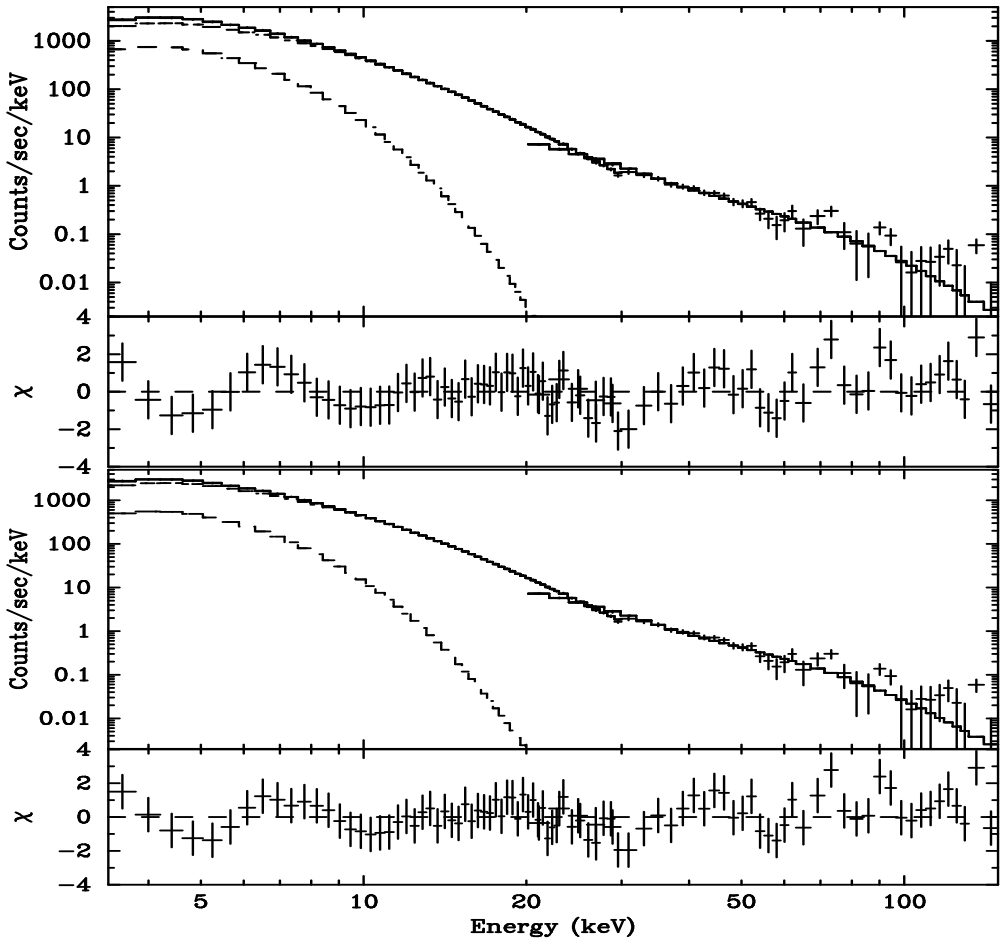

Fig. 7.— *Upper panel*: The observed spectrum in 2a with the best fit two component model consisting of CompPL and DiskBB at high electron temperature (∼5 keV) with PCA and HEXTE. PCA and HEXTE are covering the energy range of 3-30 keV and 20-150 keV, respectively. *Lower panel*: The same to the upper panel but the low electron temperature (∼0.5 keV) case.

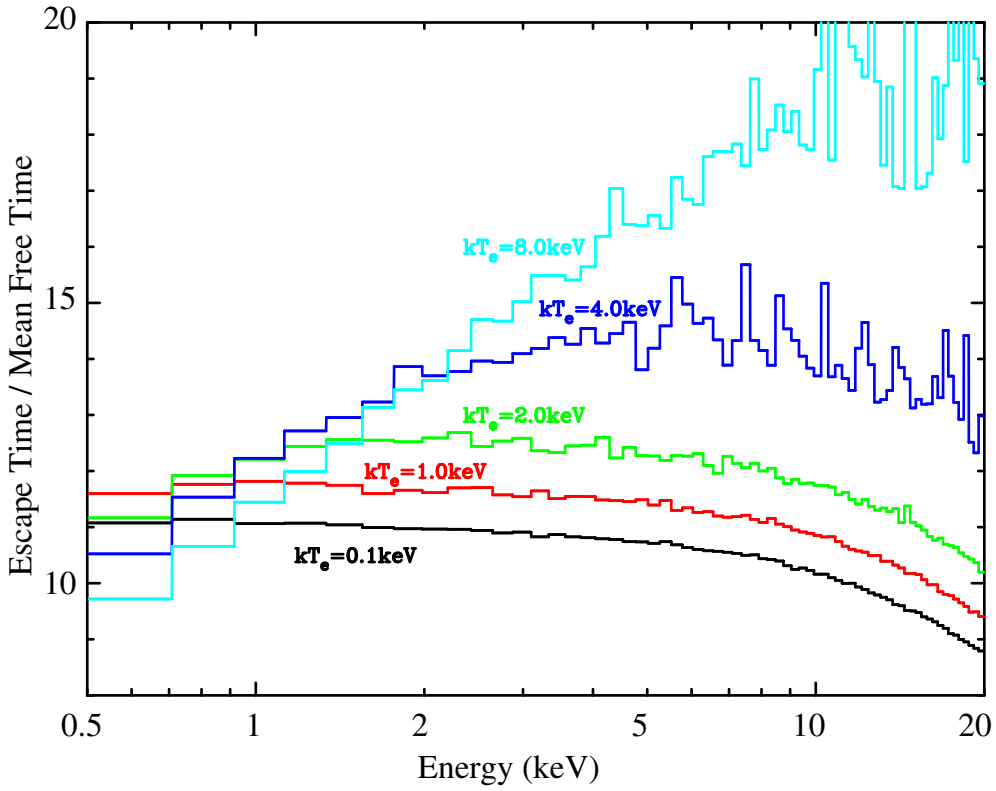

Fig. 8.— The escape time by the unit of mean free time in 0.5-20 keV estimated by the Monte Carlo simulations. The optical depth of the plasma and the power-law index of the incident photons are assumed to be 4 and -2.7, respectively. The assumed electron temperatures are indicated in the figure.

Kitamoto, & Torii 2001). The effect of the statistical fluctuation depends on the frequency. In general, the larger statistical fluctuation is included in the higher frequency region. We examined the effect of the statistical fluctuation with the Monte Carlo simulation. The real light curve in the energy range from 2 keV to 15 keV obtained by PCA in 2a is used as the time variation of the input photon source. The energy of the each photon is determined by random function, according to the power-law spectral distribution with photon index of -2.7. Since the light curve is 8 ms bin data, the photons in a bin are assumed to be produced with a fixed even interval during the bin. The emerging photons are accumulated as binned histograms with 8 ms bin for the energy bands of 2.0-2.5 keV, 2.5-3.5 keV, 3.5-7.0 keV and 7.0-15.0 keV. After excluding the transient intervals both at the start and the end of the simulation, the created light curves are analyzed as the real data and calculated the cross spectra. The example of the phase lag between 2.0-2.5 keV and 7.0-15.0 keV bands is shown in Figure **??**, where the electron temperature and the scattering optical depth are 0.1 keV and 4, and the plasma density and the radius are 3.0 $\times 10^{15}$ cm^{-3} and 2×10^{9} cm, respectively. As expected, only in the low frequency region, Figure **??** shows linear function, but in the high frequency region above 2 Hz, it shows rather large fluctuation. The actual data shown in Figure **??** have much small error. This may be due to the reason that the data include the disk component which has another coherent time variation such as QPO. If we fit the simulated lag spectrum by a linear function in the frequency range from 0 Hz to 2 Hz, the obtained delay time is 0.014 sec. This is mimicking the observed data.

3.4. *Spectral Evolution of the Class θ and the Soft Dip*

V01b and Vadawale et al. (2003) have discussed both the hard state and the soft dip. We also analyze the spectral evolution, applying the two component model consisting of DiskBB and CompPL. The light curve shown in Figure **??** is divided into 33 intervals; 26 intervals in hard state (five 100 sec intervals in each of 1a (1a1-5), 1b (1b1-5), 2a (2a1-5), 2b (2b1-5) and 3a (3a1-5), and one 150 sec interval in 3a (3a6)), two dips (100 sec interval in 1d and 135 sec interval in 2d), three post-dip intervals (125 sec in 1e1 and 1e2, and 115 sec in 2e), and two edges (50 sec intervals in 1c and 2c). Figure **??** shows the flux evolution of the two components and Figure **??** shows the best-fit parameters. The best-fit parameters are listed in Table **??**. In this analysis, we fixed $N_{\rm H}$ as 7.9×10^{22} H atoms cm^{-2} and $kT_{\rm e}$ as 0.5 keV. We found the following results; (1) The flux of CompPL is always dominant. During the dips, however, the fraction of CompPL becomes small and is roughly 2/3. (2) Except for the dips, $kT_{\rm in}$ and the normalization of CompPL positively correlate with the intensity with the smooth saw-shape. (3) The inner disk radius is consistent with a constant within the errors. (4) The index of CompPL in the dip is steeper than that in the hard state.

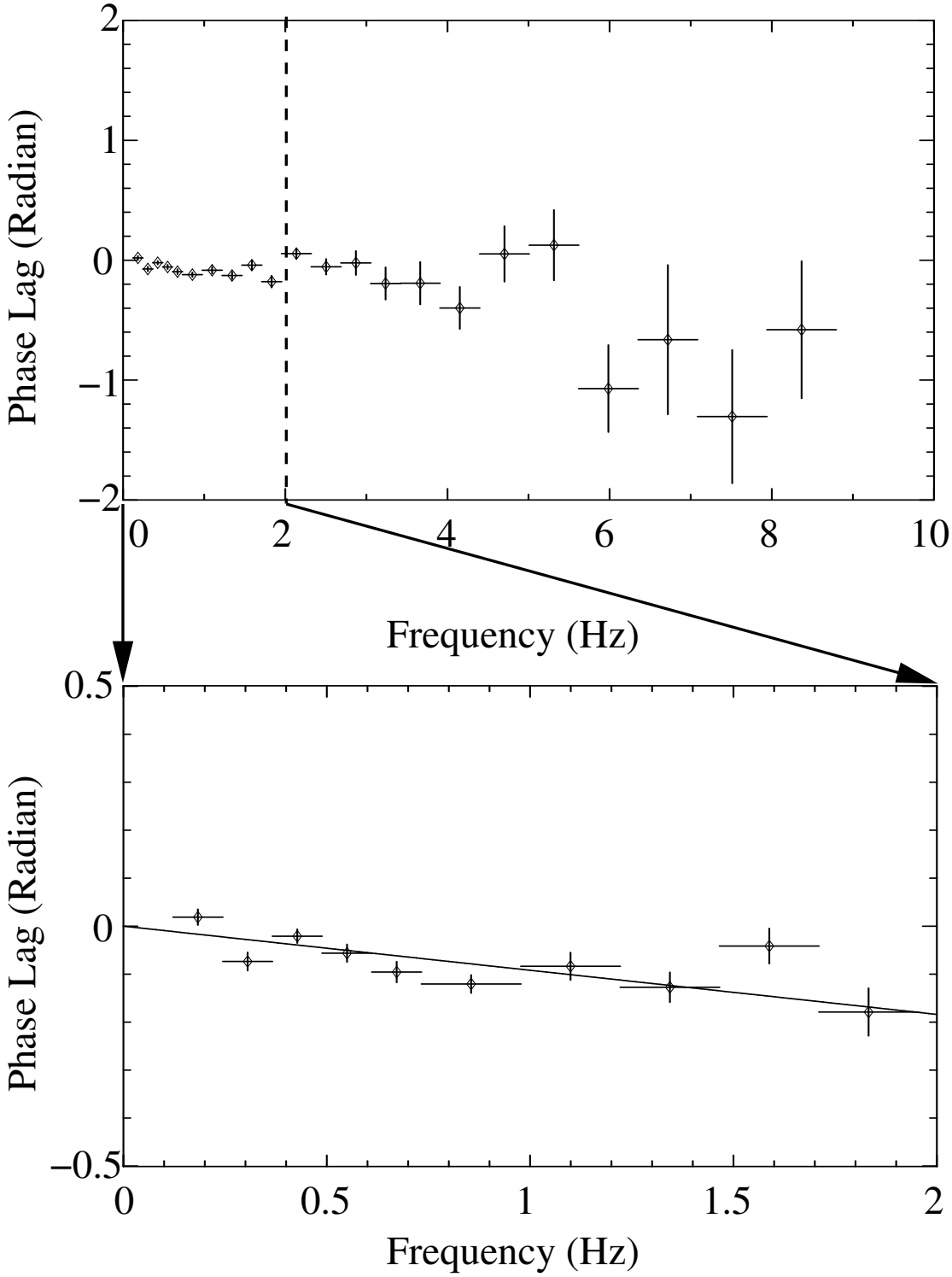

Fig. 9.— Simulation of the frequency dependence of the lag of 7-15 keV from 2-2.5 keV. The plasma is assumed to be 0.5 keV, and its radius and the density are 1.0×10^{9} cm and 3.0×10^{15} cm^{-3}. The line represents the best-fit to the results of the simulation.

Here, we note that our derived values ($r_{\rm in}$ and $T_{\rm in}$) from the DiskBB model are not reliable values because of the model is too simple and the other effects around the inner disk must be considered. However, these values have the information on the temporal change of the disk structure and the smooth continuity of the values across the dips is our notable results.

4. DISCUSSION

4.1. *Soft Lag and Compton Cloud*

We have developed a new CompPL model and applied to the spectral fittings. The observed spectra can be well fitted by the two component model. The time lag analysis shows soft lag. This soft lag can be expected by the CompPL model with $kT_e < 2$ keV as shown in Figure **??**. In the simulation, the escape time of the photons is evaluated by the unit of a mean free time of photons. Since the optical depth of the Compton cloud can be deduced by the spectral fitting as roughly 4, if we adjusted the lag time as the observed value, we can derive the size and the density of the cloud. By adjusting the simulation to the data shown in Figure **??** derived from 0 Hz to 2 Hz, the radius of the plasma is deduced to be 2×10^9 cm for the optical depth of 4. However, the derived delay time is not simple and it has a frequency dependence, because the scattering produces another statistical fluctuation and this fluctuation makes the delay effect to reduce. This effect is more efficient in the high frequency region. The simulation shown in Figure **??** is mimicking the observed frequency dependence of the delay, where the plasma is assumed to be 2×10^9 cm in the radius and the optical depth of 4 with the electron temperature of 0.1 keV. This supports the validity of the derivation of the delay time by restricting the low frequency region. Although this may not be a unique solution and there might be alternative models, our model can explain both the observed spectra and the timing behaviors. The energy dependence of the lag time is also explained as shown in Figure **??**.

The relatively low temperature of the cloud can be expected, if the cloud is exposed to the photons with the power-law spectra with the photon index of steeper than -2 down to the low energy below 1 keV. The origin of the photons (the power-law component) is still unresolved but it is considered to be an emission from the inside of the scattering cloud with the radius $\sim2\times10^9$ cm. This situation is similar to the model proposed by Nobili et al. (2000).

Our result indicates that we always observe the inner disk region. Thus, the spherical cold cloud with the optical depth of $\sim$4 can not be acceptable. If we consider the emission

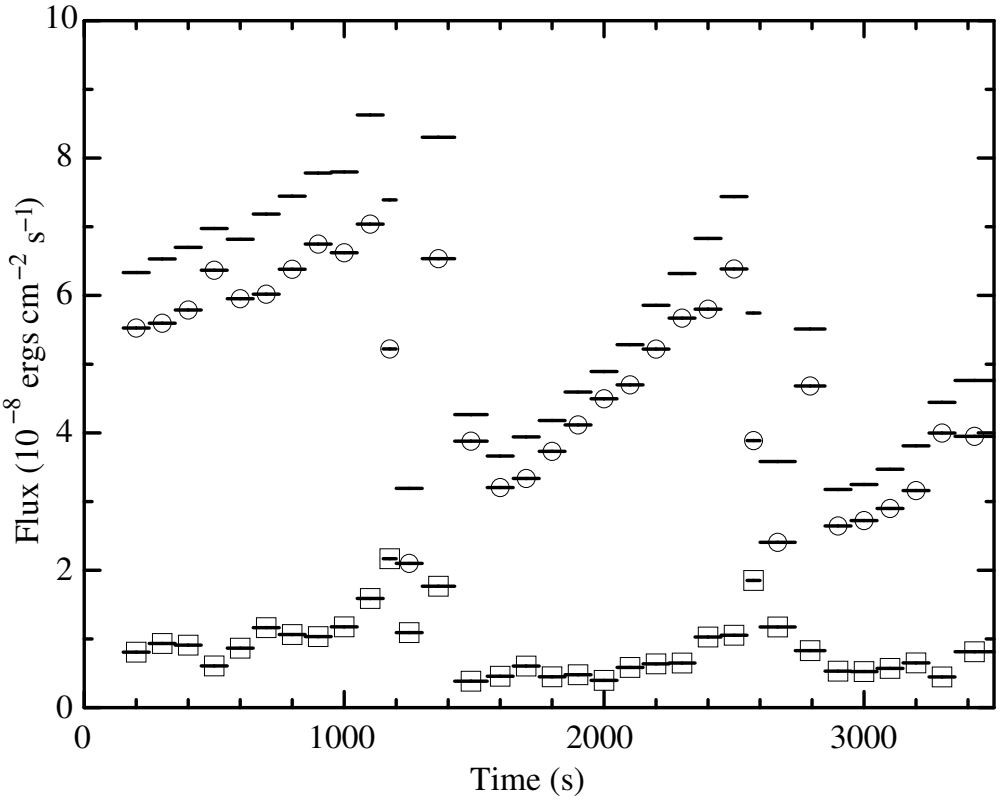

Fig. 10.— The time variation of flux. *From top to bottom*: total flux (*lines*), CompPL flux (*circles*) and DiskBB flux (*squares*).

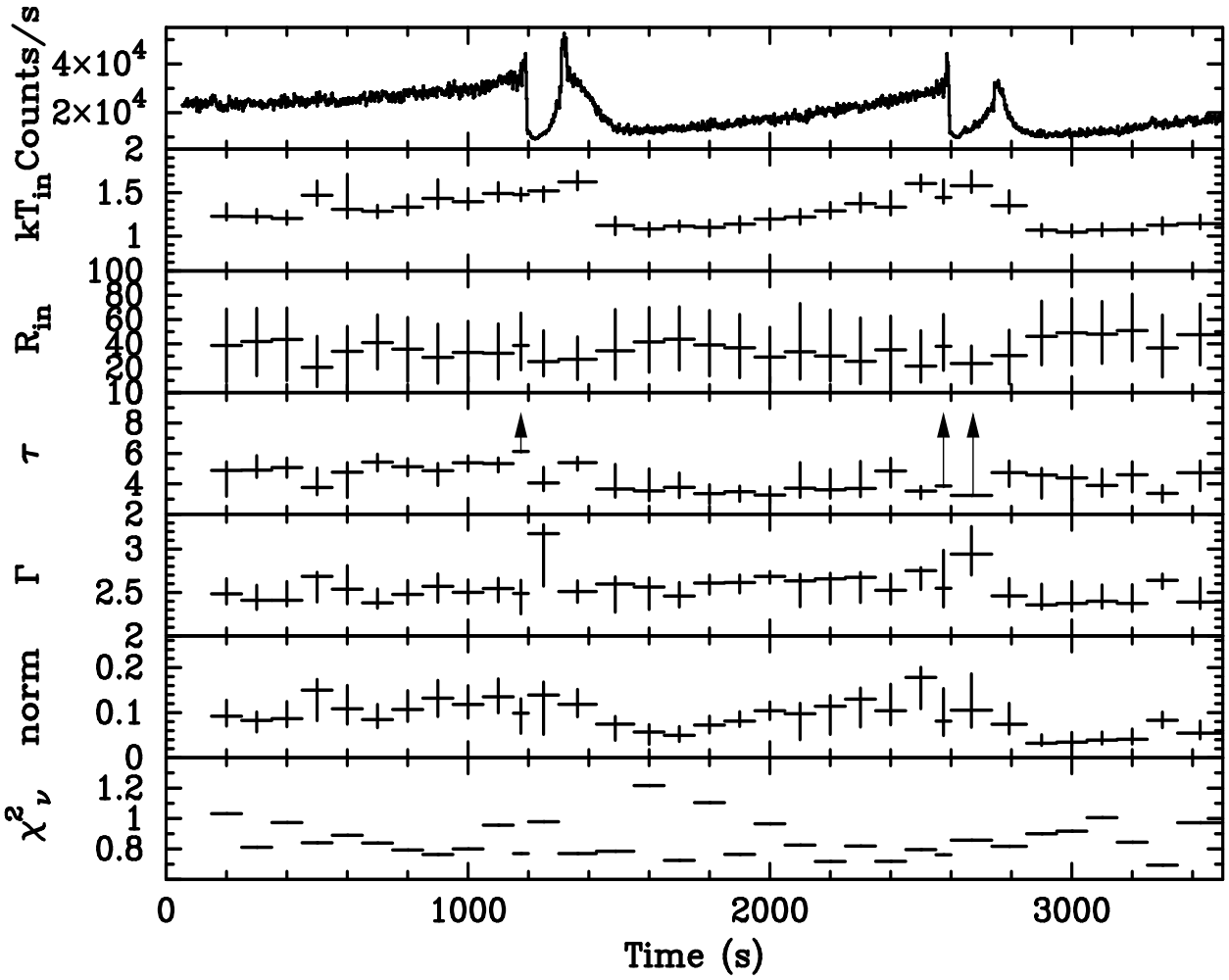

Fig. 11.— Best-fit parameters in 33 intervals. The electron temperature and the $N_{\rm H}$ are fixed at 0.5 keV and 7.9×10^{22} H atoms cm^{-2}. *From top to bottom*: PCA light curve in the energy of 2.15-15.20 keV(*first panel*); temperature at inner disk radius $kT_{\rm in}$ (*second panel*); inner disk radius $R_{\rm in}$ assuming the distance of D=9.0 kpc and inclination angle of $\theta = 70^\circ$ (*third panel*); optical depth τ (*fourth panel*); index of power-law (*fifth panel*); the normalization of the CompPL model (*sixth panel*); reduced χ^2 (*seventh panel*). Errors are 90% confidence levels, and arrows are 90% confidence lower limit.

region of the power-law component is a kind of a jet from near the black hole and extends up to $\sim 10^9$ cm (see Miyamoto & Kitamoto 1991), the scattering cloud can be considered to be the outer part of the jet itself, or surrounding gas around the jet with the radius of the order of 10^9 cm. Since the inclination angle of GRS 1915+105 is $\sim$70 deg, we may be able to observe both the inner accretion disk and the scattered hard photons originated from the jet.

The phase lag analysis of the other class has been published by Reig et al. (2000), where GRS 1915+105 does not show always soft lag, and sometimes shows hard lag in the energy range around several keV. Good correlation of the lag properties and the QPO frequency and the spectral hardness has been discovered. If the spectra are hard, the hard lag is observed. This property is preferable for the Comptonization presented here as discussed by Nobili et al. (2000), if the electron temperature is variable depending on the hardness.

4.2. *Time Evolution in the Class* θ

The parameter evolution of the two component model (DiskBB + CompPL) is shown in Figure **??**, where $N_{\rm H}$ and $kT_{\rm e}$ are fixed at 7.9×10^{22} H atoms cm^{-2} and 0.5 keV, respectively. The flux evolution of their component is shown in Figure **??**. CompPL is the major component and DiskBB is the minor component. This is a natural result because the inclination angle of GRS 1915+105 is $\sim$70 deg. The inner disk radius assuming the inclination angle of 70 deg is 21$\sim$51 km and we can not reject the constant radius during this observation. Since we used the simple disk model, DiskBB, the derived values of $r_{\rm in}$ and $T_{\rm in}$ are not true. The actual values must be different and it depends on the various effects, such as the inner disk boundary condition, relativistic effects, the radiative transfer effects, and the geometry of the disk. For example, a high temperature and a small radius has been pointed out for some high luminosity BHCs including ULXs (Makishima et al. 2000) and this can be explained by the slim disk (Watarai, Mizuno & Mineshige 2001).

If we neglect the dips, a positive correlation can be seen between the count rate and $kT_{\rm in}$, and also the count rate and the normalization of CompPL. The saw-shape cyclic variation of these parameters is suggesting the limit cycle behavior. V01b proposed that the cause of the dip is the mass ejection from the plasma represented by the Compton component, which is the dominant one around 20 keV. Belloni et al. (1997a) interpreted the transitions between outburst and quiescence are the repetition of the evacuation and the filling of inner accretion disk, and Naik et al. (2001) interpreted dips are caused by mass ejection due to the evacuation of the matter from the accretion disk. The continuity of the disk and other parameters before and after the dips shown in our analysis does not support the simple mass

ejection from the accretion disk during the dip. Our results indicate that the accretion disk and also the emission region of the power-law component do not change during the dip, and actual change occurs at the saw shape transition. The cause of the dip is a phenomenon at the outer portion than the plasma which is responsible to both CompPL and DiskBB.

One possible speculation of the dips is a transit of a scattering cloud between us and the plasma contributing the power-law or the CompPL component. The power-law component is assumed to be the emission from the jet ejected from near the black hole. During the dips, matter is ejected from somewhere, whose X-ray emission is not dominant, for example the Two Component Advection Flow (TCAF) proposed by Nandi et al, (2001). Thus, the accretion disk component does not change during the dips. However, if the ejected matters transit between the jet and observers, the CompPL component must be affected. During the dip, the normalization of CompPL does not change significantly, but the power-law index changes. In the second dip, the optical depth could be large. Considering the relation between the optical depth and the photon index of the CompPL model, the transit of the scattering matter could make the observed properties of the CompPL component. If the matter transit with 10^9 cm sec^{-1}, covering the jet with 10^9cm radius, the 3×10^{19} g sec^{-1} plasma ejection makes the electron scattering optical depth of roughly 1 and may significantly affect the spectral shape.

After the dip, the mass accretion rate in the optically thick disk once becomes small because of refilling the ejected matter and consequently the optically thick disk becomes cool and the jet emitting power-law component becomes small. Then, the mass accretion rate in the optically thick disk gradually increases, the disk temperature becomes high and the jet flows up. These successive behaviors may make the saw-shape cyclic variation.

We would like to thank the members of the *RXTE* team. This research has made use of data obtained through the High Energy Astrophysics Science Archive Research Center Online Service, provided by the NASA/Goddard Space Flight Center. Y.O. gratefully acknowledges the financial support of the Rikkyo University Special Fund for Research. S.K. gratefully acknowledges the financial support of the Grant-in-Aid for scientific Research (Grant Nos. 4654039 and 14654047).

REFERENCES

Belloni, T., Klein-Wolt, M., Méndez, M., van der Klis, M., & van Paradijs, J. 2000, A&A, 355, 271 (B00)

Belloni, T., Méndez, M., King, A. R., van der Klis, M., & van Paradijs, J. 1997a, ApJ, 479, L145

Belloni, T., Méndez, M., King, A. R., van der Klis, M., & van Paradijs, J. 1997b, ApJ, 488, L109

Bradt, H. V., Rothschild, R. E., & Swank, J. H. 1993, A&AS, 97, 355

Castro-Tirado, A. J., Brandt, S., & Lund, N. 1992, IAU Circ., 5590

Chapuis, C., & Corbel, S. 2004, A&A, 414, 659

Fender, R. P., Garrington, S. T., McKay, D. J., Muxlow, T. W. B., Pooley, G. G., Spencer, R. E., Stirling, A. M., & Waltman, E. B. 1999, MNRAS, 304, 865

Greiner, J., Cuby, J. G., & McCaughrean, M. J. 2001a, Nature, 414, 522

Greiner, J., Cuby, J. G., McCaughrean, M. J., Castro-Tirado, A. J., & Mennickent, R. E. 2001b, A&A, 373, L37

Harlaftis, E. T., & Greiner, J. 2004, A&A, 414, L13

Kohmura, T., Kitamoto, S., & Torii, K. 2001, ApJ, 562, 943

Kotani, T., Ebisawa, K., Dotani, T., Inoue, H., Nagase, F., Tanaka, Y., & Ueda, Y. 2000, ApJ, 539, 413

Lin, D., Smith, I. A., Liang, E. P., & Böttcher, M. 2000, ApJ, 543, L141

Makishima, K., Kubota, A., Mizuno, T., Ohnishi, T., Tashiro, M., Aruga, Y., Asai, K., Dotani, T., Mitsuda, K., Ueda, Y., Uno, S., Yamaoka, K., Ebisawa, K., Kohmura, Y., & Okada, K. 2000, ApJ, 535, 632

Markwardt, C. B., Swank, J. H., & Taam, R. E. 1999, ApJ, 513, L37

Migliari, S., & Belloni, T. 2003, A&A, 404, 283

Mirabel, I. F., Dhawan, V., Chaty, S., Rodríguez, L. F., Martí, J., Robinson, C. R., Swank, J., & Geballe, T. R. 1998, A&A, 330, L9

Mirabel, I. F., & Rodríguez, L. F. 1994, Nature, 371, 46

Mitsuda, K., Inoue H., Koyama, K., Makishima, K., Matsuoka, M., Ogawara, Y., Shibazaki, N., Suzuki, K., Tanaka, Y., & Hirano, T. 1984, PASJ, 36, 741

Miyamoto, S., & Kitamoto, S. 1991, ApJ, 374, 741

Miyamoto, S., Kitamoto, S., Mitsuda, K., & Dotani, T. 1988, Nature, 336, 450

Morgan, E. H., Remillard, R. A., & Greiner, J. 1997, ApJ, 482, 993

Muno, M. P., Morgan, E. H., & Remillard, R. A. 1999, ApJ, 527, 321

Naik, S., Agrawal, P. C., Rao, A. R., Paul, B., Seetha, S., & Kasturirangan, K. 2001, ApJ, 546, 1075

Nandi, A., Chakrabarti, S. K., Vadawale, S. V., & Rao, A. R. 2001, A&A, 380, 245

Nobili, L., Turolla, R., Zampieri, L., & Belloni, T. 2000, ApJ, 538, L137

Rao, A. R., Naik, S., Vadawale, S. V., & Chakrabarti, S. K. 2000, A&A, 360, L25

Rau, A., Greiner, J., & McCollough, M. L. 2003, ApJ, 590, L37

Reig, P., Belloni, T., van der Klis, M., Méndez, M., Kylafis, N., & Ford, E. C. 2000, ApJ, 541, 883

Sunyaev, E. A., & Titarchuk, L. 1980, A&A, 86, 121

Vadawale, S. V., Rao, A. R., & Chakrabarti, S. K. 2001a, A&A, 372, 793

Vadawale, S. V., Rao, A. R., Naik, S., Yadav, J. S., Ishwara-Chandra, C. H., Pramesh Rao, A., & Pooley, G. G. 2003, ApJ, 597, 1023

Vadawale, S. V., Rao, A. R., Nandi, A., & Chakrabarti, S. K. 2001b, A&A, 370, L17 (V01b)

van der Klis, M., Hasinger, G., Langmeier, A., van Paradijs, J., & Lewin, W. H. G. 1987, ApJ, 319, L13

Watarai, K., Mizuno, T., & Mineshige, S. 2001, ApJ, 549, L77

Table 2. PHASE LAG AND TIME LAG

Regions	Intervals (s)	$E_{\rm min}$ (keV)	$E_{\rm max}$ (keV)	Phase lag / Frequency (10^{-2} Radian/Hz)[a]	Time lag (ms)[b]
1a	500	5.04	6.72	-0.7±0.3	-1.1±0.4
		6.72	9.25	-2.0±0.3	-3.2±0.4
		9.25	15.20	-5.8±0.3	-9.2±0.5
1b	500	5.04	6.72	-1.8±0.6	-2.8±0.9
		6.72	9.25	-0.3±0.3	-0.5±0.5
		9.25	15.20	-2.0±0.4	-3.2±0.6
2a	500	5.04	6.72	-4.3±0.4	-6.9±0.6
		6.72	9.25	-6.4±0.4	-10.2±0.7
		9.25	15.20	-10.3±0.5	-16.4±0.8
2b	500	5.04	6.72	-1.8±0.3	-2.9±0.5
		6.72	9.25	-2.6±0.3	-4.2±0.5
		9.25	15.20	-8.0±0.4	-12.7±0.6
3a	650	5.04	6.72	-3.0±0.3	-4.8±0.6
		6.72	9.25	-7.3±0.4	-11.7±0.6
		9.25	15.20	-12.1±0.5	-19.2±0.7
1d + 2d[c]	225	5.88	9.25	-5.8±1.1	-9.2±1.7
		9.25	15.20	-2.1±1.4	-3.3±2.3

Note. — Errors are 1σ confidence levels.

[a]Lags are calculated with respect to the energy of 2.15-5.04 keV of the hard states and with respect to the energy of 2.15-5.88 keV of the dips (1d + 2d).

[b]Time lag (ms) = Phase lag (Radian) / {$2\pi\times$Frequency (Hz)}

[c]Combine two dips to increase photon number

Table 3. BEST-FIT PARAMETERS OF THE TWO COMPONENT MODEL, CONSISTING OF COMPPL AND DISKBB.

Regions	$kT_{\rm in}$[a] (keV)	$R_{\rm in}$[b] (km)	τ[c]	Γ[d]	norm[e] (10^{-2})	χ^2 (d.o.f)	2-60 keV Flux $F_{\rm total}$	$F_{\rm diskbb}$	$F_{\rm comppl}$ (10^{-8} ergs s^{-1})
1a1	$1.23^{+0.14}_{-0.04}$	39±30	$4.89^{+0.56}_{-1.70}$	$2.48^{+0.18}_{-0.12}$	$9.2^{+3.5}_{-2.2}$	90 (87)	6.33	0.81	5.53
2	$1.23^{+0.08}_{-0.07}$	42^{+27}_{-28}	$4.90^{+0.95}_{-0.47}$	$2.41^{+0.17}_{-0.11}$	$8.3^{+1.9}_{-2.5}$	71 (87)	6.53	0.93	5.60
3	$1.20^{+0.09}_{-0.07}$	44^{+26}_{-34}	$5.07^{+0.63}_{-0.64}$	$2.41^{+0.21}_{-0.06}$	$8.7^{+3.8}_{-1.8}$	85 (87)	6.70	0.91	5.79
4	$1.47^{+0.16}_{-0.11}$	21^{+26}_{-16}	$3.76^{+1.28}_{-0.47}$	$2.69^{+0.05}_{-0.29}$	$15.0^{+2.3}_{-6.8}$	73 (87)	6.98	0.61	6.37
5	$1.31^{+0.40}_{-0.10}$	34^{+21}_{-32}	$4.76^{+0.63}_{-1.65}$	$2.54^{+0.27}_{-0.17}$	$10.8^{+5.2}_{-3.4}$	77 (87)	6.82	0.87	5.95
1b1	1.29±0.07	41^{+23}_{-22}	$5.43^{+0.52}_{-0.58}$	$2.38^{+0.16}_{-0.06}$	$8.5^{+3.4}_{-1.8}$	73 (87)	7.18	1.16	6.02
2	$1.33^{+0.14}_{-0.09}$	36±26	$5.12^{+0.53}_{-0.59}$	$2.48^{+0.16}_{-0.11}$	$10.7^{+4.2}_{-2.7}$	69 (87)	7.45	1.06	6.38
3	$1.43^{+0.22}_{-0.11}$	29^{+27}_{-21}	$4.87^{+0.47}_{-0.97}$	$2.57^{+0.14}_{-0.18}$	$13.2^{+4.0}_{-4.1}$	66 (87)	7.78	1.03	6.75
4	$1.40^{+0.15}_{-0.09}$	33^{+26}_{-24}	$5.38^{+0.45}_{-0.55}$	$2.50^{+0.14}_{-0.13}$	$11.8^{+4.2}_{-3.0}$	70 (87)	7.80	1.18	6.62
5	$1.49^{+0.13}_{-0.09}$	32^{+24}_{-21}	$5.33^{+0.37}_{-0.55}$	$2.55^{+0.12}_{-0.15}$	$13.5^{+4.0}_{-3.6}$	83 (87)	8.63	1.59	7.04
1c	1.48±0.07	39^{+27}_{-20}	≥ 6.13[f]	$2.49^{+0.15}_{-0.24}$	$9.9^{+3.2}_{-4.5}$	67 (87)	7.39	2.17	5.22
1d	$1.52^{+0.05}_{-0.12}$	25^{+25}_{-12}	$4.06^{+1.03}_{-0.50}$	$3.18^{+0.10}_{-0.60}$	$13.9^{+2.9}_{-8.7}$	86 (88)	3.19	1.09	2.10
1e1	$1.62^{+0.12}_{-0.09}$	27^{+18}_{-17}	$5.40^{+0.36}_{-0.50}$	2.51±0.12	$11.8^{+3.3}_{-2.8}$	67 (87)	8.30	1.77	6.54
2	$1.12^{+0.09}_{-0.11}$	34^{+34}_{-23}	$3.66^{+1.62}_{-0.54}$	$2.60^{+0.08}_{-0.32}$	$7.5^{+1.7}_{-3.6}$	68 (87)	4.27	0.39	3.88
2a1	$1.08^{+0.07}_{-0.08}$	42^{+28}_{-25}	$3.53^{+1.45}_{-0.63}$	$2.56^{+0.10}_{-0.26}$	$5.7^{+1.6}_{-2.7}$	106 (87)	3.66	0.46	3.20
2	1.12±0.06	44^{+27}_{-25}	$3.77^{+0.94}_{-0.67}$	$2.46^{+0.16}_{-0.13}$	$5.0^{+1.9}_{-1.4}$	63 (87)	3.94	0.61	3.34
3	$1.10^{+0.08}_{-0.10}$	39^{+28}_{-25}	$3.36^{+0.58}_{-0.66}$	$2.61^{+0.09}_{-0.13}$	$7.2^{+2.0}_{-1.7}$	96 (87)	4.18	0.45	3.73
4	$1.14^{+0.09}_{-0.10}$	39^{+27}_{-25}	$3.48^{+0.37}_{-0.63}$	$2.62^{+0.09}_{-0.12}$	$8.1^{+2.1}_{-1.2}$	67 (87)	4.59	0.48	4.12
5	1.20±0.12	29^{+24}_{-21}	$3.27^{+0.54}_{-0.56}$	$2.69^{+0.06}_{-0.08}$	$10.4^{+2.0}_{-1.9}$	84 (87)	4.89	0.40	4.50
2b1	$1.22^{+0.09}_{-0.08}$	34^{+40}_{-23}	$3.72^{+1.68}_{-0.60}$	$2.63^{+0.08}_{-0.30}$	$9.8^{+2.3}_{-5.8}$	72 (87)	5.28	0.59	4.70
2	$1.29^{+0.10}_{-0.09}$	30^{+38}_{-20}	$3.61^{+1.34}_{-0.55}$	$2.66^{+0.06}_{-0.28}$	$11.4^{+2.4}_{-6.2}$	62 (87)	5.86	0.64	5.22
3	$1.37^{+0.12}_{-0.10}$	26^{+36}_{-18}	$3.70^{+1.78}_{-0.54}$	$2.68^{+0.06}_{-0.29}$	$13.0^{+2.5}_{-6.2}$	71 (87)	6.32	0.65	5.67
4	$1.33^{+0.19}_{-0.09}$	35±28	$4.85^{+0.84}_{-1.06}$	$2.53^{+0.18}_{-0.16}$	$10.4^{+5.9}_{-3.1}$	63 (87)	6.83	1.03	5.80
5	$1.61^{+0.10}_{-0.09}$	22^{+29}_{-13}	$3.53^{+0.30}_{-0.50}$	$2.75^{+0.03}_{-0.22}$	$17.8^{+2.3}_{-6.9}$	69 (87)	7.44	1.05	6.39
2c	$1.45^{+0.20}_{-0.06}$	38^{+26}_{-20}	≥ 3.86[f]	$2.55^{+0.44}_{-0.22}$	$8.1^{+7.2}_{-3.2}$	66 (87)	5.74	1.85	3.89
2d	$1.58^{+0.17}_{-0.08}$	24^{+14}_{-16}	≥ 3.23[f]	$2.94^{+0.32}_{-0.24}$	$10.5^{+8.1}_{-3.8}$	76 (88)	3.58	1.17	2.41
2e	$1.35^{+0.17}_{-0.08}$	30^{+21}_{-23}	$4.74^{+0.76}_{-0.90}$	$2.46^{+0.20}_{-0.12}$	$7.4^{+4.6}_{-2.2}$	71 (87)	5.51	0.83	4.68
3a1	1.07±0.07	46^{+29}_{-23}	$4.58^{+0.44}_{-1.52}$	$2.36^{+0.24}_{-0.05}$	$3.2^{+1.9}_{-0.5}$	78 (87)	3.18	0.53	2.65
2	$1.05^{+0.09}_{-0.05}$	49^{+28}_{-27}	$4.39^{+0.80}_{-1.51}$	$2.38^{+0.25}_{-0.09}$	$3.5^{+2.2}_{-0.8}$	80 (87)	3.25	0.53	2.72
3	$1.07^{+0.08}_{-0.07}$	48^{+27}_{-24}	$3.90^{+1.06}_{-0.72}$	$2.40^{+0.19}_{-0.08}$	$3.9^{+1.8}_{-0.9}$	88 (87)	3.47	0.57	2.90
4	$1.07^{+0.07}_{-0.06}$	51^{+30}_{-25}	$4.60^{+0.85}_{-1.13}$	$2.38^{+0.21}_{-0.09}$	$4.1^{+2.3}_{-1.1}$	74 (87)	3.81	0.65	3.16
5	$1.13^{+0.09}_{-0.10}$	37^{+27}_{-24}	$3.37^{+0.52}_{-0.57}$	$2.64^{+0.07}_{-0.09}$	$8.3^{+1.8}_{-1.7}$	60 (87)	4.44	0.45	4.00
6	$1.14^{+0.10}_{-0.06}$	48^{+25}_{-25}	$4.73^{+0.77}_{-1.18}$	$2.39^{+0.27}_{-0.08}$	$5.5^{+2.7}_{-1.3}$	85 (87)	4.76	0.81	3.95

Note. — Errors are 90% confidence levels for a single parameter.

[a]temperature at inner disk radius

[b]inner disk radius. $R_{\rm in}$ is derived from distance D=9.0 kpc and inclination angle $\theta = 70°$.

[c]optical depth of the Compton cloud

[d]index of power-law

[e]the normalization of CompPL

[f]These are the 90% lower limits.